Determining the moment of inertia tensor of a UAV using a motion capture system

D. Yang, S. Al-Zubaidi, K. Stol*
University of Auckland, 20 Symonds Street, Auckland

http://www.imavs.org/

ABSTRACT

This article proposes a novel method for finding the mass moment of inertia of a small Unmanned Aerial Vehicle (UAV). The method relies on a motion capture system to record the orientation of the object-under-test oscillating from a compound pendulum. The novelty is that it determines the location of the centre of mass and the full inertia tensor from the same set of experiments. The motion capture system records the object-under-test orientation when it is stationary and oscillating from the pendulum. By doing this for multiple orientations, the process can accurately determine the location of the centre of mass to $\pm 2mm$ error and the full moment of inertia tensor of the object to an average 3.4% error for objects with inertia in the order of $10^{-2} kgm^2$.

1 INTRODUCTION

Mass moment of inertia (MoI) is crucial in many dynamical systems, such as robotic manipulators, aerospace vehicles, and automotive systems. For UAV systems, MoI significantly impacts their flight dynamics and stability. It affects how the UAV responds to external disturbances and changes in attitude. Accurate estimation of UAV attitude is crucial for optimizing UAV performance, ensuring precise control, and achieving desired flight characteristics.

Many methods have been developed to derive the MoI of rigid bodies, including the tabulating method, Computer-Aided Design (CAD) based methods, and pendulum methods. The tabulating method is one of the most straightforward methods that estimate MoI. By tabulating each constituent's inertia as a simplified geometric shape and summing them together with respect to the principle axes while assuming symmetry, a quick and simple model is developed [1, 2]. However, this oversimplification often neglects many complex-shaped components and does not account for products of inertia.

The CAD-based method improves upon the tabulating method by allowing computers to estimate a more comprehensive list of complex components' MoI [3]. However, any deviation in manufacturing of the UAV from the CAD model, such as imperfect placement of components, results in inaccuracies.

Empirical methods account for these imperfections by directly calculating the MoI of the final product. The most prominent are the torsional and compound pendulum methods.

The torsional pendulum method involves suspending the object of interest on a platform using two or more cables and then twisting it to produce a torsional oscillation, commonly known as bifilar, trifilar, etc., pendulum. The period of oscillation is recorded to determine the MoI of the object about the rotating axis. Although accurate measurements have been achieved with this method [4, 5, 6, 7], its setup can be time-consuming as the placement of the complex object axis needs to align with the platform's throughout the oscillation period. Additionally, complex objects may require additional "ad hoc" support for each measurement when particular axes are to be measured [7]. This additional material further complicates the experiments.

On the other hand, the compound pendulum method suspends the object from a pivot point and measures its unforced swinging period. NASA has employed this method to accurately determine the MoI of various aircraft to $< 2.5\%$ error as early as 1934 [8]. However, this often requires multiple accurate and expensive sensors placed at various locations on the object [9]. More recently, other combinations of measurement instruments have been employed, such as using an inclinometer for obtaining the period of oscillation [10]. However, the authors comment that the instrument is only suitable for measuring slow oscillations; the fast changes result in underestimating the angle, requiring an additional marker-based motion-capturing system to achieve accurate measurements.

These methods rely on the simple principle where a component of gravitational force supplies a constant torque to the system, giving rise to the oscillatory motion. Under the assumption of small angles, it becomes a second-order undamped system. By accurately measuring the period of oscillation, the MoI for that pivot axis can be derived.

However, these methods have limitations, including the reliance on the small angle assumption and undamped oscillation. It should be noted that the dynamics of a simple pendulum motion is a well-explored problem [11, 12, 13]; the damping effect due to both the aerodynamic and structure can be accurately modelled even for large angles.

Furthermore, the major limitation of these methods is the requirement to know the centre of mass (CoM) of the object-

*Email address(es): kstol@auckland.ac.nz

http://www.imavs.org/

under-test. For instance, the trifilar pendulum necessitates the accurate placement of the object's CoM on the vertical line passing through the rotational centre of the platform. Any misplacement can lead to undesired translations of the entire system, thereby compromising the accuracy of the results. Estimating the CoM can be challenging, particularly for complex-shaped or multi-component objects.

This article proposes a novel method that addresses the abovementioned challenges and provides an accurate and practical solution for measuring MoI in complex-shaped or multi-component objects without requiring precise CoM estimation. This approach takes advantage of the sub-millimetre accuracies of a motion capture system which many laboratories around the world share.

The rest of the paper is organised as follows. Section 2 discusses the high-level approach for this method, followed by a closer examination of system modelling in section 3. Then section 4 describes the experimental setup. The experimental data are analysed and the results discussed in section 5. Finally, the paper concludes and discusses future work in section 6.

2 METHODOLOGY

The fundamental idea follows that of a traditional compound pendulum. The object-under-test, e.g. a MAV, hanging from the pendulum is displaced from its stationary position. Its angular motion is then recorded to derive its MoI.

However, the novelty lies in that the object can be hung from any point on its rigid body in any orientation, and the CoM location is determined in the same experiments as MoI simultaneously using a motion capture system (MoCap). The ideas behind determining both properties are as follows.

When an object is hung from a pendulum with a lightweight pivot arm, Its CoM naturally lies below the pivot axis on the vertical plane. By placing the object in various orientations, multiple planes on which the CoM lies can be obtained. Then its position in 3D can be calculated by finding the intersection of all the planes.

A full inertia tensor can be obtained from the oscillation data of various unique orientations. These orientations do not have to be on the principle axes of the object (I_{xx}, I_{yy}, I_{zz}); they can be arbitrary. Each orientation gives us an MoI value about a specific axis. With at least six unique axis values, the full tensor can be derived using linear regression.

The Experimental procedure is explained below:

1. Rigidly attach the object to a pivot arm in an arbitrary orientation. This is the attachment point and object orientation is denoted as one configuration.

2. Start recording this configuration when it is stationary. Allow some time to record this stationary configuration, e.g. 5s, as this stationary data will be used for deriving the location of CoM.

3. When satisfied, give a small displacement to the object such that it oscillates freely for at least 10 periods. This is to allow the MoCap system to capture enough data for processing later. This part of the data (dynamic data) will be used for MoI calculation.

4. After the recording, create a new configuration by hanging it at a different orientation. Note that it is crucial that this new orientation is unique, i.e. not linearly dependent on the previous ones, otherwise, it results in a duplicate measurement of MoI about an already-measured axis.

5. Repeat the steps for at least six recordings for obtaining a full tensor. Additional testing reduces the error of final results.

To process the data, a flow chart describing the high-level process is shown in figure 1. Three groups of data from MoCap are obtained. D_{static} denotes the static data where the system is stationary when hanging freely on a pendulum. D_{rig} and $D_{dynamic}$ are both the dynamic oscillatory data after the system is displaced from its stable equilibrium position; D_{rig} consists of only the pivot arm in oscillation.

The CoM of the object can be obtained with at least $N = 3$ of D_{static} data, where N is the number of experiments conducted. Once the CoM is determined, its distance to the pivot axis can be calculated for each experiment. These distances, in addition to the MoI of the pivot arm obtained from D_{rig} and the MoI of the system from $D_{dynamic}$, can isolate the MoI about an axis through its CoM of the object alone. Then these MoI values are transformed to the full inertia tensor about a set of axes the users defines fixed to the object. Note that at least $N = 6$ is needed since the full inertia tensor has 6 unique values. With this, both the CoM and MoI tensor are derived.

3 THEORY

This section discusses the notations and equations used for calculating both the CoM and MoI of the object.

The object-under-test is denoted as O, the pivot arm that rigidly connects the pivot axis and the object-under-test as A, and the combined system in oscillation S, such that the mass of the combined system m_S is

$$m_S = m_O + m_A \tag{1}$$

where m_O and m_A are the mass of the object and pivot arm, respectively.

3.1 Coordinate frames

Three coordinate frames are defined: world frame $\{W\}$, object frame $\{O\}$, and the pivot arm frame $\{A\}$. Figure 2 visualises the relationship between the frames.

$\{O\}$ is fixed to the body of the object-under-test; its orientation in $\{W\}$ varies from experiment to experiment depending on how the object is attached. The CoM of the object in

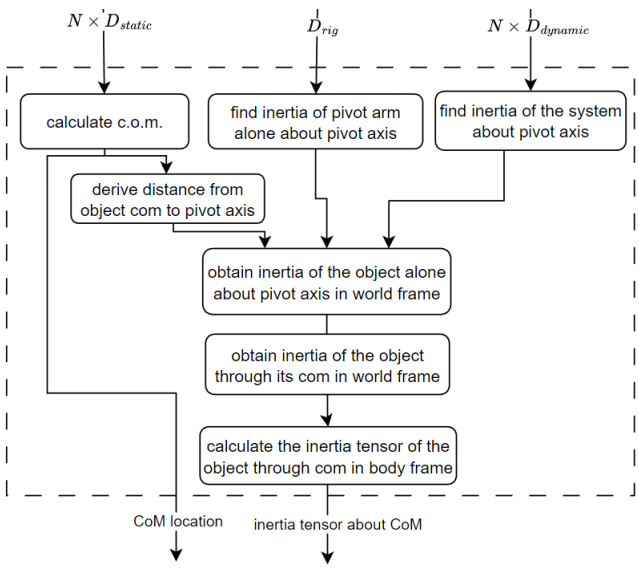

Figure 1: Data processing procedural flowchart, showing the high-level general steps taken towards calculating a rigid body's CoM and MoI

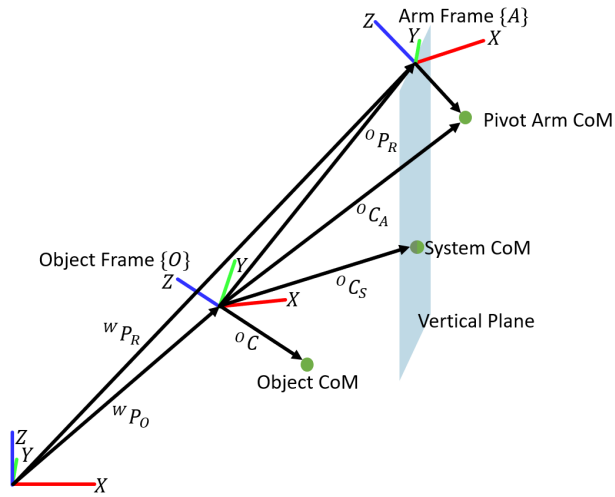

Figure 2: Coordinate Frames. Object frame {O} is fixed to the body of the object-under-test in an arbitrary orientation. Arm frame {A} rotates with the pivot arm; its origin sits on the pivot axis; its y axis aligns with the pivot axis at all times.

the object frame ${}^{O}\mathbf{c}$ is unknown but constant throughout all experiments. The pivot arm frame $\{A\}$ is fixed to the pivot arm. Its origin lies at the bearing centre such that its y axis is the pivot axis, which both the object-under-test and the pivot arm oscillate about. $\{A\}$ rotates with the pivot arm. Figure 2 shows a case where the pivot arm's CoM is not directly between the object CoM and the pivot axis. Note that the system CoM always lies directly on the vertical plane below the pivot axis when at rest.

The position of CoM is denoted as $\mathbf{c}$, and other positions are denoted as $\mathbf{p}$. The distance to CoM of a specific item, such as the overall system, S, is noted as $\mathbf{c}_S$; the coordinate frame such measurement is in is noted as ${}^{W}\mathbf{c}$ in the case of the world frame. For example, ${}^{O}\mathbf{p}_A$ denotes the position of the arm frame origin in the object frame; ${}^{A}\mathbf{c}$ denotes the position of the pivot arm's CoM in the arm frame.

The transformation matrices $\mathbf{T}$ of world-to-object ${}^{O}_{W}\mathbf{T}$ and world-to-rig ${}^{R}_{W}\mathbf{T}$ can be defined as

$$ {}^{i}_{W}\mathbf{T} = \begin{bmatrix} {}^{i}_{W}\mathbf{R}_{\,3\times3} & -{}^{W}\mathbf{p}_{i\;3\times1} \\ 0\;0\;0 & 1 \end{bmatrix}_{4\times4} \tag{2} $$

where $i \in \{O, R\}$, e.g. ${}^{O}_{W}\mathbf{R}$ is the rotation matrix from world to object frame.

3.2 Centre of Mass

To find the object CoM location ${}^{O}\mathbf{c}$, two points on the same plane satisfy the relationship

$$ {}^{O}\hat{\mathbf{n}}^{T}\,{}^{O}\mathbf{c}_S = {}^{O}\hat{\mathbf{n}}^{T}\,{}^{O}\mathbf{p}_A \tag{3} $$

where ${}^{O}\hat{\mathbf{n}}$ is the normal vector of the vertical plane in the object frame and

$$ {}^{O}\hat{\mathbf{n}} = {}^{O}_{W}\mathbf{R}\,{}^{W}\hat{\mathbf{n}}. \tag{4} $$

The vertical plane can be set to align with a world principle axis, e.g. ${}^{W}\hat{\mathbf{n}} = [0\;1\;0]^T$.

As shown in figure 2, ${}^{O}\mathbf{p}_A$ can be derived from

$$ {}^{O}\mathbf{p}_A = {}^{O}_{W}\mathbf{R}({}^{W}\mathbf{p}_R - {}^{W}\mathbf{p}_O) \tag{5} $$

where ${}^{W}\mathbf{p}_R$ and ${}^{W}\mathbf{p}_O$ are the position of the rig and object frame origins in the world, measured by MoCap. To obtain${}^{O}\mathbf{c}_S$, the CoM equation

$$ m_t d_t = \sum_i m_i d_i \tag{6} $$

where m_t and m_i denote the total mass of the system and the mass of its constituents, is used. d_t, d_i denote the distance from the system's and its constituents' CoM to a fixed point. Since the system consist of two components: the pivot arm and the object-under-test,

$$ m_S\,{}^{O}\mathbf{c}_S = m_O\,{}^{O}\mathbf{c} + m_A\,{}^{O}\mathbf{c}_A. \tag{7} $$

Recall that m_A, m_A and m_O are the mass of the system (Eq.1), pivot arm, and object, respectively. ${}^{O}\mathbf{c}$ is the CoM position of the object to be solved for. ${}^{O}\mathbf{c}_A$ can be expressed as

$$ {}^{O}\mathbf{c}_A = {}^{O}_{W}\mathbf{R}({}^{R}_{W}\mathbf{R}^{-1}\,{}^{A}\mathbf{c} + {}^{W}\mathbf{p}_R - {}^{W}\mathbf{p}_O) \tag{8} $$

where ${}^{A}\mathbf{c} = [0,\ 0,\ -d_A]^T$, d_A is the distance from the rig's CoM to the pivot axis. d_A is measured by balancing the pivot arm on a sharp edge.

http://www.imavs.org/

http://www.imavs.org/

Substituting Eq.7 into Eq.3 gets

$$ {}^{O}\hat{\mathbf{n}}^{T}\ m_S^{-1}(m_O\ {}^{O}\mathbf{c} + m_A\ {}^{O}\mathbf{c}_A) = {}^{O}\hat{\mathbf{n}}^{T\,O}\mathbf{p}_A. \tag{9} $$

Rearranging for ${}^{O}\mathbf{c}$ yields

$$ {}^{O}\hat{\mathbf{n}}^{T\,O}\mathbf{c} = {}^{O}\hat{\mathbf{n}}^{T}({}^{O}\mathbf{p}_A - \frac{m_A}{m_S}{}^{O}\mathbf{c}_A)\frac{m_S}{m_O} \tag{10} $$

where all variables are directly measurable by the MoCap system: ${}^{O}\mathbf{c}_A$ is described by Eq.8., and ${}^{O}\mathbf{p}_A$ Eq.5.

With N experiments conducted, a system of equations is obtained as

$$ \begin{bmatrix} {}^{O}\hat{\mathbf{n}}_i^T \\ \vdots \end{bmatrix}_{N\times 3} {}^{O}\mathbf{c}_{3\times 1} = \begin{bmatrix} {}^{O}\hat{\mathbf{n}}_i({}^{O}\mathbf{p}_{A,\,i} - \frac{m_A}{m_S}{}^{O}\mathbf{c}_{A,\,i})\frac{m_S}{m_O} \\ \vdots \end{bmatrix}_{N\times 1} \tag{11} $$

where i denotes each of the experimental data. This can be written into the standard form for a system of linear equations $\mathbf{Ax} = \mathbf{b}$, and can solve for $\mathbf{x}$ by finding the pseudoinverse $\mathbf{A}^{\dagger}$, yielding

$$ {}^{O}\mathbf{c} = \begin{bmatrix} {}^{O}\hat{\mathbf{n}}_i^T \\ \vdots \end{bmatrix}^{\dagger} \begin{bmatrix} {}^{O}\hat{\mathbf{n}}_i({}^{O}\mathbf{p}_{A,\,i} - \frac{m_A}{m_S}{}^{O}\mathbf{c}_{A,\,i})\frac{m_S}{m_O} \\ \vdots \end{bmatrix}. \tag{12} $$

Thus, the least-square error value of ${}^{O}\mathbf{c}$ is found given the experimental data.

3.3 Moment of Inertia Tensor

To calculate the MoI of an object on a compound pendulum, the equation of motion is

$$ {}^{W}I_S\ddot{\theta} + \tau_d + m_s g d_s sin\theta = 0 \tag{13} $$

where ${}^{W}I_S$ is the MoI of the system about the pivot axis, θ is the angle of oscillation, $m_s g$ is the gravitational force, and d_s is the distance from the system's CoM to the pivot axis. The τ_d term denotes the damping torque experienced by the system due to both aerodynamics and bearing friction [11]

$$ \tau_d = a\dot{\theta} + b\dot{\theta}^2 sgn\left(\dot{\theta}\right) \tag{14} $$

where a, b are the damping constants Combing Eq.13 and 14 then rearranging to have

$$ \ddot{\theta}_k{}^{W}I_S + a\dot{\theta}_k + b\dot{\theta}_k^2 sgn(\dot{\theta}_k) = m_s g d_s sin\theta_k \tag{15} $$

where θ_k is the angle measurement from the MoCap system at time step k. From the dynamic data, a times series of $\theta_k, \dot{\theta}_k, \ddot{\theta}_k$ that can be written into matrix form can be obtained:

$$ \begin{bmatrix} \ddot{\theta}_i & \dot{\theta}_i & \dot{\theta}_i^2 sgn\dot{\theta}_i \\ \vdots & \vdots & \vdots \end{bmatrix}_{K\times 3} \begin{bmatrix} {}^{W}I_S \\ a \\ b \end{bmatrix} = m_s g d_s sin \begin{bmatrix} \theta_i \\ \vdots \end{bmatrix}_{K\times 1} \tag{16} $$

where i denotes the value at each corresponding time step and K = the total number of time steps. Solving for $[{}^{W}I_S\ a\ b]^T$ results in

$$ \begin{bmatrix} {}^{W}I_S \\ a \\ b \end{bmatrix} = m_s g_s d_s \begin{bmatrix} \ddot{\theta}_i & \dot{\theta}_i & \dot{\theta}_i^2 sgn\dot{\theta}_i \\ \vdots & \vdots & \vdots \end{bmatrix}^{\dagger} sin \begin{bmatrix} \theta_i \\ \vdots \end{bmatrix}_{K\times 1}. \tag{17} $$

The same equations apply to finding the MoI of the pivot arm about the pivot axis ${}^{W}I_A$. Once ${}^{W}I_S$ and ${}^{W}I_A$ are found, the MoI of the object through its CoM can be derived:

$$ {}^{W}I = {}^{W}I_S - {}^{W}I_A - m_o||{}^{W}\mathbf{p}_R - {}^{W}\mathbf{p}_O||^2 \tag{18} $$

where ${}^{W}I$ is the MoI of the object about an axis through its CoM in the world frame. That axis is parallel to and on the same plane as the pivot axis. $m_o||{}^{W}\mathbf{p}_R - {}^{W}\mathbf{p}_O||^2$ is the parallel axis term. With N experiments, there are N ${}^{W}I$ values.

To transform these MoI values about the arbitrary axes onto the user-defined object body frame, it can be shown that

$$ {}^{O}\hat{\mathbf{z}}^{T\,O}\mathbf{I}^{O}\hat{\mathbf{z}} = {}^{W}I \tag{19} $$

where ${}^{O}\hat{\mathbf{z}}_{3\times 1} = [x,\ y,\ z]^T$ is the directional vector describing the orientation of the pivot axis in the object frame, and ${}^{O}\mathbf{I}_{3\times 3}$ is the full inertia tensor of the object in the object frame.

For N experiments, Eq.19 can be written as

$$ \begin{bmatrix} x_i & y_i & z_i \\ \vdots & \vdots & \vdots \end{bmatrix}_{N\times 3} \begin{bmatrix} Ixx & Ixy & Ixz \\ Ixy & Iyy & Iyz \\ Ixz & Iyz & Izz \end{bmatrix} \begin{bmatrix} x_i & \dots \\ y_i & \dots \\ z_i & \dots \end{bmatrix}_{3\times N} = \begin{bmatrix} {}^{W}I_i \\ \vdots \end{bmatrix}_{N\times 1} \tag{20} $$

and expanding the LHS using a standard 2nd-order trinomial expansion yields

$$ \begin{bmatrix} x_i^2 & y_i^2 & z_i^2 & 2x_iy_i & 2x_iz_i & 2y_iz_i \\ \vdots & \vdots & \vdots & \vdots & \vdots & \vdots \end{bmatrix}_{N\times 6} \begin{bmatrix} Ixx \\ Iyy \\ Izz \\ Ixy \\ Ixz \\ Iyz \end{bmatrix} = \begin{bmatrix} {}^{W}I_i \\ \vdots \end{bmatrix}_{N\times 1} \tag{21} $$

thus solving for ${}^{O}\mathbf{I}$ yields

$$ \begin{bmatrix} Ixx \\ Iyy \\ Izz \\ Ixy \\ Ixz \\ Iyz \end{bmatrix} = \begin{bmatrix} x_i^2 & y_i^2 & z_i^2 & 2x_iy_i & 2x_iz_i & 2y_iz_i \\ \vdots & \vdots & \vdots & \vdots & \vdots & \vdots \end{bmatrix}^{\dagger} \begin{bmatrix} {}^{W}I_i \\ \vdots \end{bmatrix}. \tag{22} $$

The full tensor of the object-under-test in a frame that is fixed to the object is now derived.

4 EXPERIMENTAL SETUP

This section describes an implementation of the methodology in section 2.

For the purpose of validation, an object of known MoI is used. Shown in figure 3, the object is a Polymethyl methacrylate (PMMA) circular disk of dimension 400mm in diameter, 10mm in thickness and uniform density. The hole cutouts are for the purpose of attachment. The analytical value of the

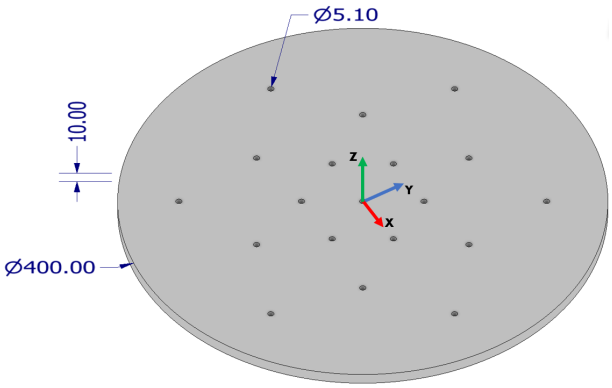

Figure 3: Circular disk PMMA. Dimensions in mm.

full inertia tensor is calculated given the radius, thickness and mass to be

$$^{O}\mathbf{I}_{analytical} = \begin{bmatrix} 1.4810 & 0 & 0 \\ 0 & 1.4810 & 0 \\ 0 & 0 & 2.9521 \end{bmatrix} \times 10^{-2} kgm^2 \tag{23}$$

which is in the same order of magnitude as a small UAV [14, 15, 16, 17]. Note that the hole cutouts are also taken into account.

The physical rig setup is shown in figure 4. Two tripods rigidly hold a steel rod horizontally above the ground. They stand a suitable distance apart such that the object-under-test can swing without obstruction. A laser pointer is used to ensure the rod is levelled. Two retro-reflective markers are put on the ends of the rod, marking the pivot axis.

The pivot arm consists of a bearing, two 3D-printed parts, and an aluminium bar. The 3D printed parts are used to rigidly attach the bar to the bearing and the object to the bar. Note that the pivot arm should be constructed in a way such that the distance from its CoM to the pivot axis can be obtained from simple methods such as balancing on a sharp edge accurately. One more marker is placed on the pivot arm such that it tracks the angular displacement of the arm.

For the object-under-test, the object frame is defined by placing 4 markers on the object, marking the origin, +x, +y and +z directions. This origin does not lie on the CoM.

For the motion capture system, VICON cameras with software VICON 3.9.0 is used for recording the object pose. An instance of the recorded objects is shown in figure 5. In the figure, the rig frame is defined such that its x-axis is the pivot axis, and the origin of the frame lies on the leftmost marker. The object frame is fixed to the object-under-test at an arbitrary pose.

Figure 4: An instance of the rig setup

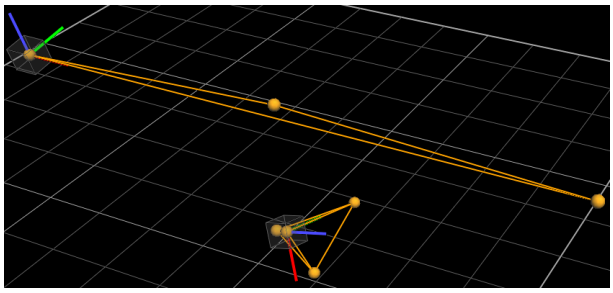

Figure 5: An example of tracked markers.

5 DATA PROCESSING AND RESULT

This section discusses the data processing and visualisation when calculating the CoM and MoI of the object, using MATLAB.

After following the steps described in section 2, VICON exports the data to a list of .csv files and is read by MATLAB. Figure 6 shows one of the experimental data sets. For at least the first 5s, the system is stationary. This section of the data is D_{static}, used for locating the object's CoM. Dynamic data $D_{dynamic}$ starts from 17s in the example in figure 6.

Transformation matrices (Eq.2) are first constructed using D_{static} for each experiment. Figure 7 shows an instance of the object rotation in the world frame (*poseplot*() function). This should reflect the orientation of the object shown in VICON. With all the transformation matrices obtained, the CoM location in the object frame can be derived by finding the point with the least distance to all the intersecting planes with Eq.3.

On the other hand, for $D_{dynamic}$, it is required to obtain the angular velocity and acceleration from the measured angle data by VICON. They are needed for Eq.17. A simple difference function is applied twice to obtain velocity and acceleration data. To resolve the issue of derivative noise amplification, a zero-phase filter function *smoothdata()* in MAT-

http://www.imavs.org/

http://www.imavs.org/

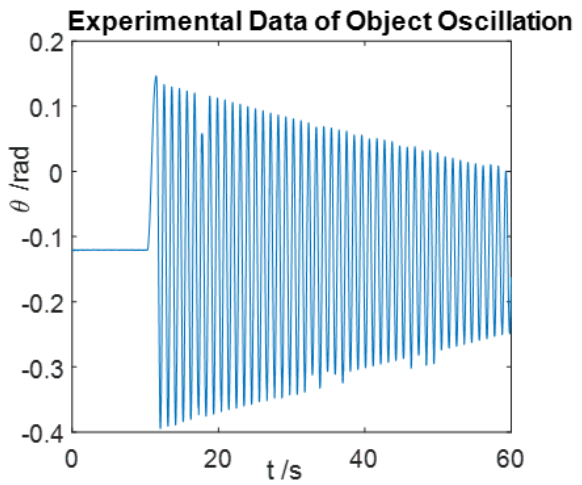

Figure 6: VICON recorded data for one experiment including both static and dynamic data

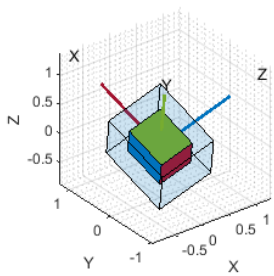

Figure 7: ${}^{O}_{W}\mathbf{R}$ visualisation for one experiment. In each experiment, the object frame has a unique orientation in the world frame.

LAB is used with the *method* parameter specified as *'sgolay'*, denoting a Savitzky-Golay filter. It is good at rejecting particularly high-frequency noise such as those from derivatives [18].

Once the kinematic data are obtained, Eq.8 is applied and finds the system MoI about the pivot axis and the two damping coefficients. The accuracy of the fitted model parameters $[I_S\ a\ b]^T$ can be verified by comparing the experimental data and model-generated data given the initial conditions

$$\begin{bmatrix}\theta_0\\ \dot{\theta}_0\end{bmatrix} = \begin{bmatrix}\theta_{peak}\\ 0\end{bmatrix}$$

where θ_{peak} denotes the angle of oscillation at a peak from the corresponding experimental data. These peaks can be found using the *findpeaks()* function in MATLAB on the filtered data. For the experiments, all the fitted models obtained above 95% match to the experimental data. Figure 9 shows an instance of the compared data.

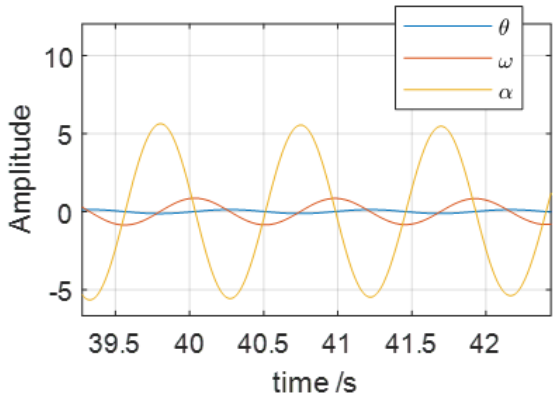

Figure 8: A segment of angle, velocity, and acceleration of the object's oscillation derived and filtered from one experimental VICON data.

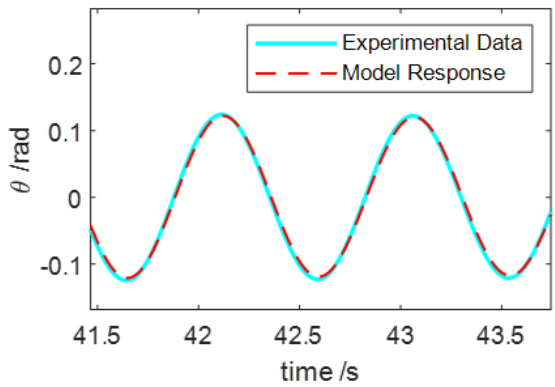

Figure 9: Model validation. By providing the same initial conditions to the fitted model, the model response can be simulated and compared to the experimental data. The figure shows a segment of a 97% match fitted model from one experiment

The CoM value is calculated as, in m,

$${}^{O}\mathbf{c} = \begin{bmatrix}-3.75\times10^{-4}\\ 4.96\times10^{-2}\\ -1.01\times10^{-2}\end{bmatrix}$$

Because an object of known geometry is used to validate the experiment, the location of the CoM can be directly measured on the object to be

$${}^{O}\mathbf{c}_{measured} = \begin{bmatrix}0\\ 5.0\times10^{-2}\\ -1.2\times10^{-2}\end{bmatrix} m$$

Both the x and y components have less than 1mm error, however, there is a 1.9mm difference in the z axis. This error becomes significant later in the MoI result.

The experimental inertia tensor of the object-under-test in the object frame ${}^{O}\mathbf{I}$ is found to be, in kgm^2,

$$ {}^{O}\mathbf{I} = \begin{bmatrix} 0.014871 & 0.00066724 & 0.00029924 \\ 0.00066724 & 0.014910 & -9.8791 \times 10^{-5} \\ 0.00029924 & -9.8791 \times 10^{-5} & 0.031907 \end{bmatrix} $$

Compared with analytical values ${}^{O}\mathbf{I}_{analytical}$, the percentage error can be calculated

$$ \%error = \begin{bmatrix} 0.8\% & - & - \\ - & 1\% & - \\ - & - & 8.2\% \end{bmatrix} $$

Averaging the percentage error on the diagonal terms to obtain an overall error percentage of 3.4%. The experimental values show good estimates in I_{xx} and I_{yy} with a low percentage error of around 1%. However, there's a larger error in I_{zz} of 8.2%; this can be traced back to inaccuracies in the derived CoM position in z, where a large error in the CoM values led to a larger inertia percentage error.

The error of 1.2mm is because there is not enough variation in the third component of the normal plane vector ${}^{O}\hat{\mathbf{n}}$ in Eq.12, i.e. the z axis angle. This made the least-square regression unable to filter out the error in this term. Physically, this means that more different angle placement about the z axis of the object relative to the vertical plane would help with the CoM calculation.

The experiment also shows good estimate about the products of inertia terms. While unable to obtain the percentage error, it can be seen that values are all in the order of magnitude $10^{-4}kgm^2$. Compare to the diagonal terms which are in the order of $10^{-2}kgm^2$, the products of inertia terms are negligible and reflects those in ${}^{O}I_{analytical}$. It is worth noting that the calculation does not treat the products of inertia differently from the main diagonal terms, and that the fact that all six value are calculated to be close to that of the analytical values demonstrates the accuracy of the method.

6 CONCLUSION

An experimental method to determine the moment of inertia tensor of a rigid body is proposed in this paper. It also calculates the object's centre of mass location relative to a body frame defined by the markers that the user attaches to the object.

For the object studied, the average percentage error across the three principle axes is calculated to be 3.4%, proving that the method is valid and that the experiments are suitable for obtaining the inertia of objects of this size. To achieve good accuracy, a wide variety of orientations that define new configurations in all three axes is desired.

Future work includes further validating the experiment with asymmetrical objects, as to determine the percentage error of the products of inertia. Additionally, more investigation can go into the sensitivity analysis of the MoI of the object-under-test to the length of the pivot arm. Experiments found that a long pivot arm increases the parallel axis term in Eq.18 which dominates the system inertia ${}^{W}I_S$, making it more difficult to obtain an accurate ${}^{W}I$.

ACKNOWLEDGEMENTS

The research reported in this article was conducted as part of "Enabling unmanned aerial vehicles (UAVs) to use tools in complex dynamic environments UOCX2104", which is funded by the New Zealand Ministry of Business, Innovation and Employment.

REFERENCES

[1] M Yasir Amir and Valiuddin Abbass. Modeling of quadrotor helicopter dynamics. In *2008 International Conference on Smart Manufacturing Application*, pages 100–105. IEEE, 2008.

[2] Randal W Beard. Quadrotor dynamics and control. *Brigham Young University*, 19(3):46–56, 2008.

[3] W Hussein, M El-khatib, A Elruby, and H Haleem. Quad rotor design, simulation and implementation. In *International Conference on Computer Science from Algorithms to Applications,(CSAA09)*, 2009.

[4] Hongwu Wang, Garrett G Grindle, Samuel Connor, and Rory A Cooper. An experimental method for measuring the moment of inertia of an electric power wheelchair. In *2007 29th Annual International Conference of the IEEE Engineering in Medicine and Biology Society*, pages 4798–4801. IEEE, 2007.

[5] Y Minami Koyama, HS Miranda, A Monrroy Cano, and B Senzio-Savino Barzellato. Experimental determination of an irregular object's moment of inertia. In *First International Congress on Instrumentation and Applied Sciences, Cancun QR Mexico*, 2010.

[6] PL Ringegni, MD Actis, and AJ Patanella. An experimental technique for determining mass inertial properties of irregular shape bodies and mechanical assemblies. *Measurement*, 29(1):63–75, 2001.

[7] Emiliano Mucchi, Stefano Fiorati, Raffaele Di Gregorio, and Giorgio Dalpiaz. Determining the rigid-body inertia properties of cumbersome systems: Comparison of techniques in time and frequency domain. *Experimental techniques*, 35(3):36, 2011.

[8] Hartley A Soule and Marvel P Miller. The experimental determination of the moments of inertia of airplanes. Technical report, 1934.

[9] NASA Armstrong Flight Loads laboratory. X-56 moment of inertia tests. https://www.youtube.com/watch?v=7xQJ2sVQrUA.

http://www.imavs.org/

[10] Roman Gabl, Thomas Davey, Edd Nixon, and David M Ingram. Accuracy analysis of the measurement of centre of gravity and moment of inertia with a swing. *Applied Sciences*, 11(12):5345, 2021.

[11] Peter F Hinrichsen. The period of the damped non-linear pendulum. *European Journal of Physics*, 41(5):055002, 2020.

[12] Kim Johannessen. An analytical solution to the equation of motion for the damped nonlinear pendulum. *European Journal of Physics*, 35(3):035014, 2014.

[13] Augusto Beléndez, Carolina Pascual, DI Méndez, Tarsicio Beléndez, and Cristian Neipp. Exact solution for the nonlinear pendulum. *Revista brasileira de ensino de física*, 29:645–648, 2007.

[14] Jemie Muliadi, Rizki Langit, and Benyamin Kusumoputro. Estimating the uav moments of inertia directly from its flight data. In *2017 15th International Conference on Quality in Research (QiR): International Symposium on Electrical and Computer Engineering*, pages 190–196. IEEE, 2017.

[15] Elisa Capello, Hyeongjun Park, Bruno Tavora, Giorgio Guglieri, and Marcello Romano. Modeling and experimental parameter identification of a multicopter via a compound pendulum test rig. In *2015 Workshop on Research, Education and Development of Unmanned Aerial Systems (RED-UAS)*, pages 308–317. IEEE, 2015.

[16] Valentin Wüest, Vijay Kumar, and Giuseppe Loianno. Online estimation of geometric and inertia parameters for multirotor aerial vehicles. In *2019 International Conference on Robotics and Automation (ICRA)*, pages 1884–1890. IEEE, 2019.

[17] Michael Burri, Janosch Nikolic, Helen Oleynikova, Markus W Achtelik, and Roland Siegwart. Maximum likelihood parameter identification for mavs. In *2016 IEEE International Conference on Robotics and Automation (ICRA)*, pages 4297–4303. IEEE, 2016.

[18] Çağatay Candan and Hakan Inan. A unified framework for derivation and implementation of savitzky–golay filters. *Signal Processing*, 104:203–211, 2014.

http://www.imavs.org/